

# High-Resolution Climate Risk Modeling for Coastal Zones Using an Innovative Downscaling Technique

Heri Sulistiyono<sup>1,\*</sup>, I Wayan Yasa<sup>1</sup>, Eko Pradjoko<sup>1</sup>, Dewandha Mas Agastya<sup>1</sup>,  
M. Ari Firdaos<sup>1</sup>, Bing Chen<sup>2</sup>

<sup>1</sup>Department of Civil Engineering, University of Mataram, Indonesia

<sup>2</sup>Department of Civil Engineering, Memorial University of Newfoundland, Canada

Received October 21, 2025; Revised March 4, 2026; Accepted March 26, 2026

## Cite This Paper in the Following Citation Styles

(a): [1] Heri Sulistiyono, I Wayan Yasa, Eko Pradjoko, Dewandha Mas Agastya, M. Ari Firdaos, Bing Chen, "High-Resolution Climate Risk Modeling for Coastal Zones Using an Innovative Downscaling Technique," *Civil Engineering and Architecture*, Vol. 14, No. 3, pp. 1509 - 1519, 2026. DOI: 10.13189/cea.2026.140309.

(b): Heri Sulistiyono, I Wayan Yasa, Eko Pradjoko, Dewandha Mas Agastya, M. Ari Firdaos, Bing Chen (2026). *High-Resolution Climate Risk Modeling for Coastal Zones Using an Innovative Downscaling Technique*. *Civil Engineering and Architecture*, 14(3), 1509 - 1519. DOI: 10.13189/cea.2026.140309.

Copyright©2026 by authors, all rights reserved. Authors agree that this article remains permanently open access under the terms of the Creative Commons Attribution License 4.0 International License

**Abstract** Coastal communities face mounting threats from climate-induced disasters, driven by rising sea levels and intensifying hydrometeorological extremes. This study introduces a reproducible, high-resolution downscaling framework that integrates numerical extrapolation, regression analysis, and artificial neural networks (ANN) to assess future coastal hazard scenarios. The approach combines the interpretability of regression with the nonlinear pattern-recognition capabilities of ANN, enabling robust projections of inland tidal inundation and extreme rainfall under IPCC AR6 CMIP6 scenarios (historical 1994–2020; SSP2-4.5 and SSP5-8.5 to 2100). Inputs include bias-corrected regional climatology, station and reanalysis records (1994–2024), local hydrometeorological observations, drainage maps, population and infrastructure layers, and the 6 July 2025 flood event for calibration. Ensemble selection, quantile-mapping bias correction, and hybrid regression-ANN modeling, are used to preserve linear relationships while capturing complex interactions. Methods include correlation-based indicator selection, cross-validated training with RMSE and MAE metrics, numerical flood simulations, and geospatial hazard-exposure-vulnerability mapping. Applied to Ampenan, West Nusa Tenggara, the framework projects inland tidal flooding up to 300 meters and rainfall intensities exceeding 3,000 mm, validating its utility for localized risk assessment. Outputs include ensemble-median projections with 5–95% uncertainty

ranges and prioritized adaptation recommendations, including structural reinforcements, ecosystem-based buffering, and early-warning systems. The framework is replicable and scalable, offering a transparent tool for climate-informed planning across diverse coastal contexts. Limitations include data resolution and evolving land-use dynamics, which may affect long-term accuracy. Practically, the model supports municipal planning, infrastructure investment, and targeted interventions for vulnerable populations. Socially, it enhances inclusive risk communication and community preparedness. By bridging statistical and machine learning techniques, this study contributes a novel methodology for disaster risk assessment and strengthens resilience in the face of accelerating climate change.

**Keywords** Coastal Disasters, Climate Change, Downscaling Methodology, Hybrid Regression-ANN, Ampenan Coastal Area

---

## 1. Introduction

Climate change has far-reaching environmental, social, and economic consequences [1–3]. It drives rising temperatures, shifting precipitation patterns, and intensifies extreme weather events such as storms and

cyclones [2]. These changes disrupt ecosystems, threaten biodiversity, and challenge human societies [2]. In particular, coastal regions face heightened risks due to sea level rise, saltwater intrusion, tidal flooding, and erosion caused by melting polar ice caps and glaciers [3,4]. These impacts endanger infrastructure, homes, and livelihoods, especially in low-lying and densely populated coastal communities [2,3,5,6].

The vulnerability of coastal areas is compounded by the degradation of natural protective ecosystems, such as mangroves, coral reefs, and wetlands, which reduces resilience against storm surges and limits resources for local economies [4]. Coastal industries, including fisheries, tourism, and trade, are increasingly exposed to climate-related disruptions [4]. For example, the Ampenan Coastal area in Indonesia has experienced severe abrasion due to rough winds and high waves, damaging dozens of homes and threatening community safety [6]. These challenges underscore the urgent need for localized climate adaptation and disaster risk reduction strategies.

While numerous studies have examined the environmental impacts of climate change, fewer have integrated hydrometeorological and geospatial data to assess disaster risk with sufficient granularity and predictive robustness [7–9]. Existing models often lack the resolution or contextual sensitivity required for effective local planning. Technical gaps persist in downscaling global climate data to regional contexts, particularly in areas with limited infrastructure and complex environmental variability. Moreover, there is a pressing need for predictive indicators that can reliably inform mitigation and preparedness efforts at the community level.

This study introduces a hybrid downscaling method that combines regression analysis with artificial neural networks (ANN). Regression provides interpretability but is limited to linear relationships, often underfitting complex disaster contexts. ANN, by contrast, captures nonlinear patterns and learns from large datasets, making it well-suited for climate risk assessment. By integrating global climate data with local hydrological records, disaster archives, and geospatial information, the approach enhances flood risk modeling for the Ampenan Coastal area. The analysis applies correlation and regression techniques, ANN training, numerical modeling, and geospatial mapping [7–9].

**The primary objectives of this research are:**

- To develop and validate a context-sensitive downscaling technique for regional climate risk analysis
- To identify key indicators that influence disaster likelihood in coastal zones
- To advance predictive modeling approaches by integrating regression analysis and artificial neural networks

By examining Lombok Island’s Ampenan Coast as a

representative equatorial region, this study shows how global climate trends translate locally. The results improve disaster risk modeling accuracy and provide a replicable framework to support climate-informed decisions in vulnerable coastal areas [4].

## 2. Materials and Methods

This study uses a three-stage methodological framework to evaluate the impacts of climate change and disaster risks in coastal communities. It integrates global climate data, local observations, and participatory assessments. As shown in Figure 1, the workflow consists of the following stages: (1) data collection, (2) data analysis and modeling, and (3) synthesis and dissemination.

### 2.1. Stage 1: Data Collection

#### 2.1.1. Global Climate Data Acquisition

Global climate variables were sourced from the World Data Center for Climate (WDCC) [<https://www.wdc-climate.de/ui/>], focusing on CMIP6 outputs under RCP 4.5 and RCP 8.5 scenarios. Monthly gridded data for temperature, precipitation, and sea level rise were extracted and interpolated to match the study region using bilinear interpolation.

#### 2.1.2. Local Climate Observations

This study utilizes long-term local climate records to support the development and validation of the proposed downscaling methodology. The observational data include daily measurements of key meteorological variables such as rainfall, temperature, humidity, and wind speed. These datasets undergo standard preprocessing procedures, such as outlier detection, normalization, and quality control, to ensure consistency and reliability for modeling purposes. The processed data are then integrated into the broader analytical framework, which combines statistical techniques and machine learning algorithms to enhance regional climate risk assessment.

Details regarding data sources, specific preprocessing steps, and regional characteristics are presented in the case study section to contextualize the application of the method.

#### 2.1.3. Disaster Incident Records

Disaster data were collected through structured interviews and field observations. Events such as tidal flooding, erosion, and infrastructure damage were geotagged and logged annually.

#### 2.1.4. Topographic Data

Topographic data were acquired via field surveys using theodolites and waterpasses, producing elevation contours and slope gradients.

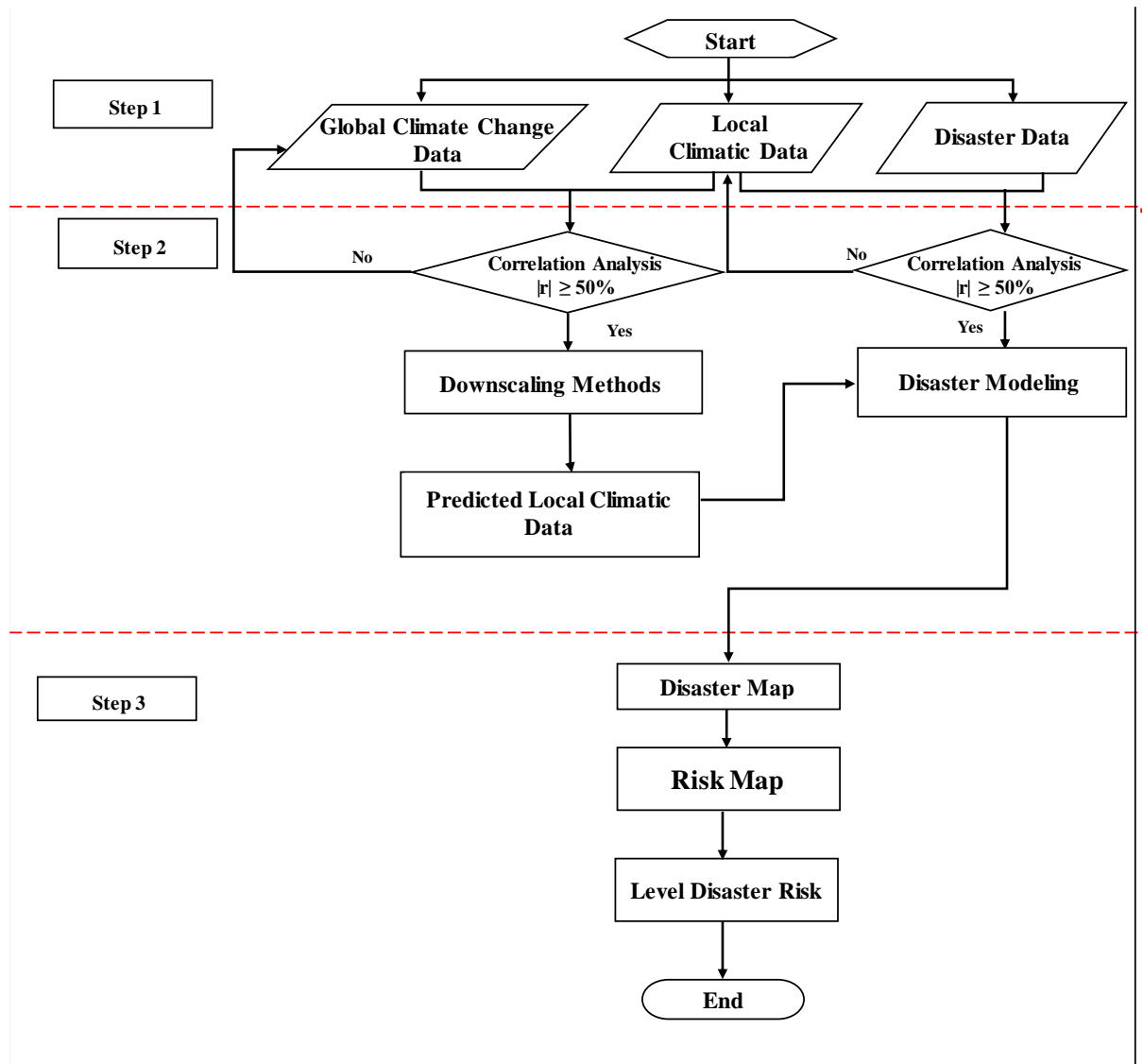


Figure 1. Workflow of the research

## 2.2. Stage 2: Data Analysis and Modeling

### 2.2.1. Statistical Downscaling

Statistical downscaling is a statistical modeling technique used to convert the coarse resolution of global climate change variables into the fine resolution of local climate change variables. This modeling involves variable screening analysis and regression modeling [10-12].

### 2.2.2. Variable Screening Analysis

Variable screening analysis was used to identify global climate change variables associated with local observations. A hybrid approach combining Pearson's correlation and Artificial Neural Networks (ANNs) was adopted to overcome the limitations of linear analysis and leverage the strengths of machine learning. Pearson correlation detects linear relationships but is sensitive to outliers and less effective for complex climate data. ANNs, by contrast, capture nonlinear interactions, identify

important predictors, and are more robust to noise and multicollinearity. This hybrid method combines the interpretability of classical statistics with the flexibility of machine learning, resulting in more accurate and comprehensive analyses of rainfall, wind, and flooding interactions.

The ANNs were configured with a single hidden layer containing up to 80 neurons, optimized regionally for complexity and efficiency. The model employed the Adam optimizer with a fixed learning rate of 0.001, and sigmoid activation functions were used for both hidden and output layers. Training was performed over 1,000 epochs with a batch size of 32. To ensure generalization, the dataset was split into 70% training, 15% validation, and 15% testing. This unified architecture provided moderate predictive accuracy across diverse coastal regions, supporting the identification of key climate predictors while maintaining methodological transparency and reproducibility.

Global variables were filtered based on their correlation

with local climate variables. Only those with an absolute Pearson correlation coefficient above 0.5 were retained [10-12]:

$$r_{xy} = \frac{n \sum x_i y_i - (\sum x)(\sum y)}{\sqrt{(n \sum x_i^2 - (\sum x)^2)(n \sum y_i^2 - (\sum y)^2)}} \quad (1)$$

with:  $r$  is the Pearson's correlation coefficient,  $n$  is the number of data,  $x$  is the global climate change variable, and  $y$  is the local disaster variable.

Artificial Neural Networks (ANNs) are advanced nonlinear regression models, with the most common architecture being backpropagation. A typical network includes input, output, and hidden layers, sometimes more than one, as in one model that required 139 hidden layers to achieve an  $R^2$  of 0.80. ANNs identify key climate predictors but do not present explicit equations; instead, the trained network must be saved and reused. Nevertheless, ANNs offer deterministic output and efficiently capture complex nonlinear relationships in climate data.

### 2.2.3. Disaster Intensity Modeling

In this paper, disaster intensity is modeled using a hybrid approach that combines regression and artificial neural networks. The model was then expressed as:

$$y = a_0 + a_1 x_1 + a_n x_n + ANNs(x_1, x_n) + \epsilon \quad (2)$$

with:  $y$  is the local disaster variable,  $x$  is the global climate change variable,  $ANNs(x_1, x_n)$  is the artificial neural networks model of  $x_1, x_n$ , and  $\epsilon$  is the residual errors.

Equation (2) represents the hybrid regression - ANN formulation, where the regression component provides the linear baseline estimate of the disaster intensity, expressed as  $y = a_0 + a_1 x_1 + a_n x_n$ . The ANN component, denoted as  $ANN(x_1, x_n)$ , models the nonlinear residuals and complex interactions among predictors that are not captured by the regression term. The final prediction is obtained by superimposing the regression output and the ANN output, such that:

$$y = y_{reg} + y_{ANN} + \epsilon.$$

where  $y_{ANN} = ANN(x_1, x_n)$  and  $\epsilon$  represents unexplained residual error. This formulation ensures that the regression term maintains interpretability by quantifying direct linear contributions of climate variables, while the ANN term enhances predictive skill by capturing nonlinear dependencies. The combination thus balances transparency and accuracy, allowing the model to reproduce both simple and complex climate-disaster relationships.

Model performance was evaluated using Root Mean Square Errors [10-12] as

$$RMSE = \left( \frac{\sum (y_i - \hat{y})^2}{n} \right)^{1/2} \quad (3)$$

with: RMSE is the Root Mean Square Error,  $y_i$  is the predicted variable,  $\hat{y}$  is the observed value, and  $n$  is the number of data set.

### 2.2.4. Flood Simulation

In this research, river flooding and inundation zones were simulated using the HEC-RAS model. The process begins with rainfall projections, typically derived from downscaled climate models such as CMIP6. These projections inform a hydrological model, such as HEC-HMS, which generates runoff hydrographs for the target watershed. The resulting runoff data are then imported into HEC-RAS, which simulates river flow and floodplain behavior [13]. Cross-sectional profiles, digital elevation models (DEMs), and land use data are used to model river geometry. Boundary conditions, including upstream inflow and downstream water levels, are established using hydrological outputs and historical records. HEC-RAS then performs unsteady flow simulations to capture the dynamic development of flood waves. HEC-RAS model parameters must be adjusted before use. Model validation is critical and involves using data from previous flood events to calibrate the model and verify its accuracy. Once validated, HEC-RAS can simulate future flood scenarios. This integrated approach identifies vulnerable areas and informs climate-resilient adaptation strategies.

## 2.3. Stage 3: Demonstration of Use

### 2.3.1. Case Study Location

The project is located in the Ampenan Coastal Area, as shown in Figure 2.

### 2.3.2. Climate Change Data

Climate change refers to long-term shifts in temperatures and weather patterns, mainly caused by human activities like burning fossil fuels. To derive data, visit sources like the World Data Center for Climate (WDCC) or the Copernicus Climate Data Store and download datasets using filters or APIs. The steps to retrieve data are as follows:

1. Open the WDCC (World Data Center for Climate) website.
2. Log in and register your account.
3. Open the "Search" page.
4. Select a variation.
5. Download the data.

Available data includes: Air Temperature, Relative Humidity, Wind Speed, Eastward Wind, Specific Humidity, Water Evaporation Flux, Cloud Area Fraction, Surface Temperature, and Sea Water Salinity.



**Figure 2.** Case Study Location

2.3.3. Local Rainfall Data

The Rescaled Adjusted Partial Sums (RAPS) technique is used to evaluate the consistency of time series data, such as rainfall records, by analyzing cumulative deviations from the mean. By rescaling partial sums, RAPS effectively highlights anomalies or structural shifts, which aid in the detection of inhomogeneities. This method is commonly applied in hydrological studies and supports the validation of long-term climate and precipitation datasets. In this research, it was implemented at five monitoring stations: Dasan Cermen, Geres Daya, Gunung Sari, Keru, and Serumbung.

The results of the consistency test using RAPS indicate that the data from the five stations are homogeneous.

2.3.4. Correlation Analysis

Table 1 presents the correlation analysis results between rainfall measurements from local stations and GCM variables with a correlation coefficient of 50% or higher. Predictor selection retained variables with Pearson correlation coefficients of  $r \geq 0.5$ . This threshold is consistent with established practices in climate downscaling, where medium correlations are considered sufficient to capture meaningful associations between large-scale predictors and local climate variables [14,15]. While higher thresholds may exclude relevant predictors, adopting  $r \geq 0.5$  balances statistical strength with physical interpretability, ensuring robust yet inclusive variable screening.

**Table 1.** The Correlation Analysis

Station	Pearson's Correlation			ANNs		
	Air Temp.	Wind Speed	Eastward. Wind	Surf. Temp.	Surf. Temp.	Clo Ar Fract.
Ds Cermen	0.50	-0.50	0.58	0.59	0.641	0.341
Gr Daya	-	-0.53	0.66	0.57	0.412	0.515
Gn Sari	-	-	0.51	0.50	0.257	0.679
Keru	-	-0.50	0.54	0.51	0.185	0.663
Serumbung	-	-	0.54	0.50	0.374	0.552

2.3.5. Disaster Modeling

The final results of the climate change-based disaster models show that for storm data at five stations: Dasan Cermen, Geres Daya, Gunung Sari, Keru, and Sembung, they are:

$$R = -25155 + 84.9*AT + 27.76*EW + ANN(ST,CAF) + E$$

With  $r = 0.643$  and  $RMSE = 115.079$

$$R = -6968 + 17.32*EW + 23.5*ST + ANN(ST,CAF) + E$$

With  $r = 0.651$  and  $RMSE = 61.921$

$$R = -17428 + 15.76*EW + 58.3*ST + ANN(ST,CAF) + E$$

With  $r = 0.567$  and  $RMSE = 96.566$

$$R = -16224 + 25.22*EW + 54.5*ST + ANN(ST,CAF) + E$$

With  $r = 0.58267$  and  $RMSE = 120.862$

$$R = -13779 + 15.94*EW + 46.2*ST + ANN(ST,CAF) + E$$

With  $r = 0.473$  and  $RMSE = 97.249$

2.3.6. Rainfall Prediction

The rainfall predictions for five stations until the year 2100 are shown in the following five figures.

Figures 3 to 7 present the annual rainfall predictions for five different rainfall stations under the high-resolution downscaling scenario for the period 2018–2118. Each figure shows the time series of annual rainfall (y-axis, in

mm) plotted against simulation years (x-axis). The highest predicted yearly rainfall occurs at the Dasan Cermen Station (Figure 3), estimated to be around 3000 mm. The Keru Station (Figure 4) follows with a maximum annual rainfall of 2130 mm, Gunung Sari Station (Figure 5) at 1700 mm, Serumbung Station (Figure 6) at 1640 mm, and Geres Daya Station (Figure 7) with a maximum of 1080 mm.

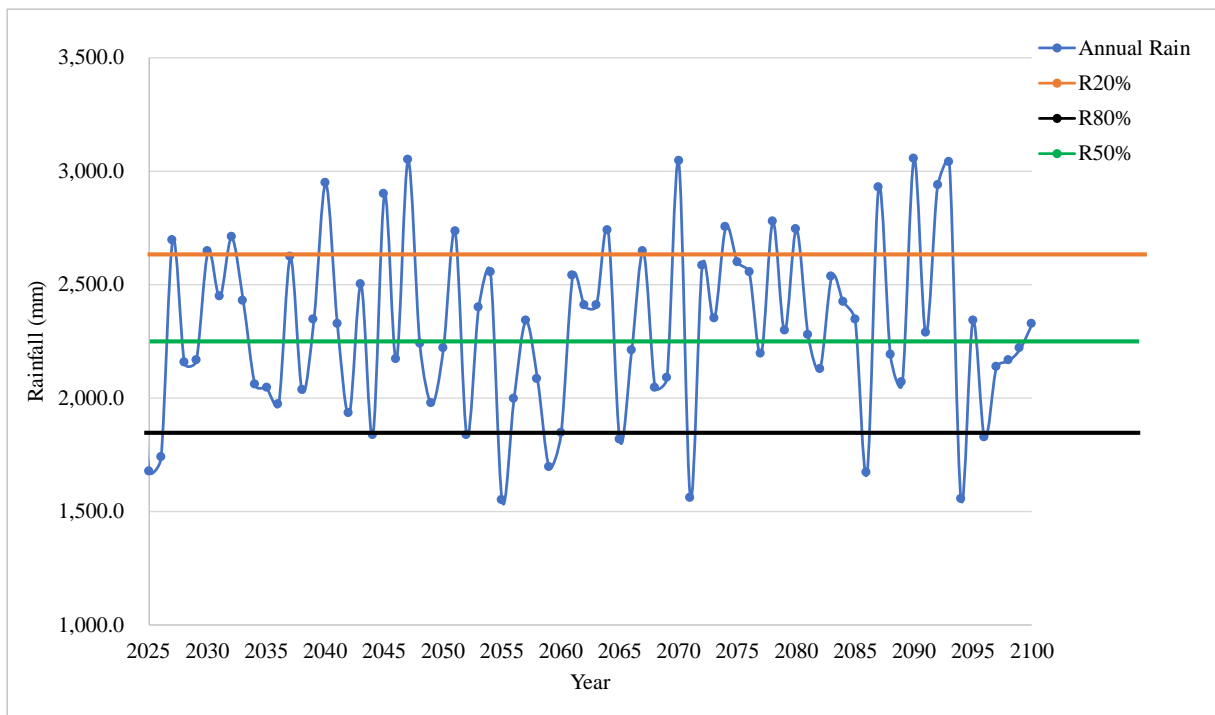


Figure 3. Predicted Rainfall in the Dasan Cermen Station

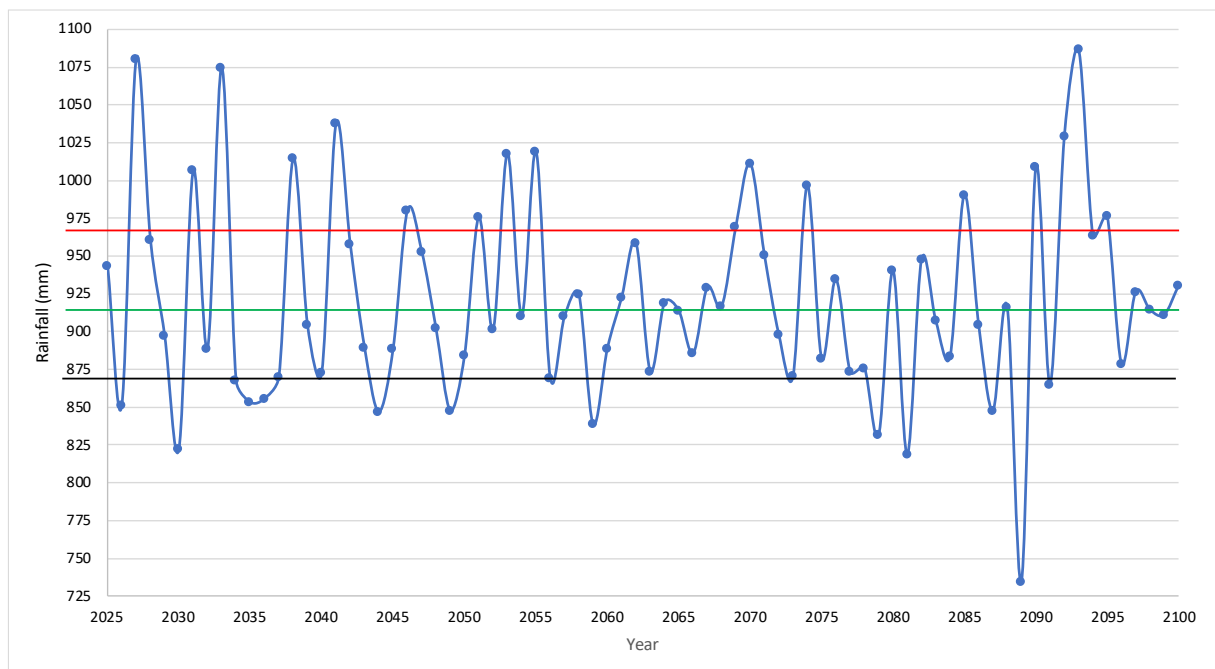
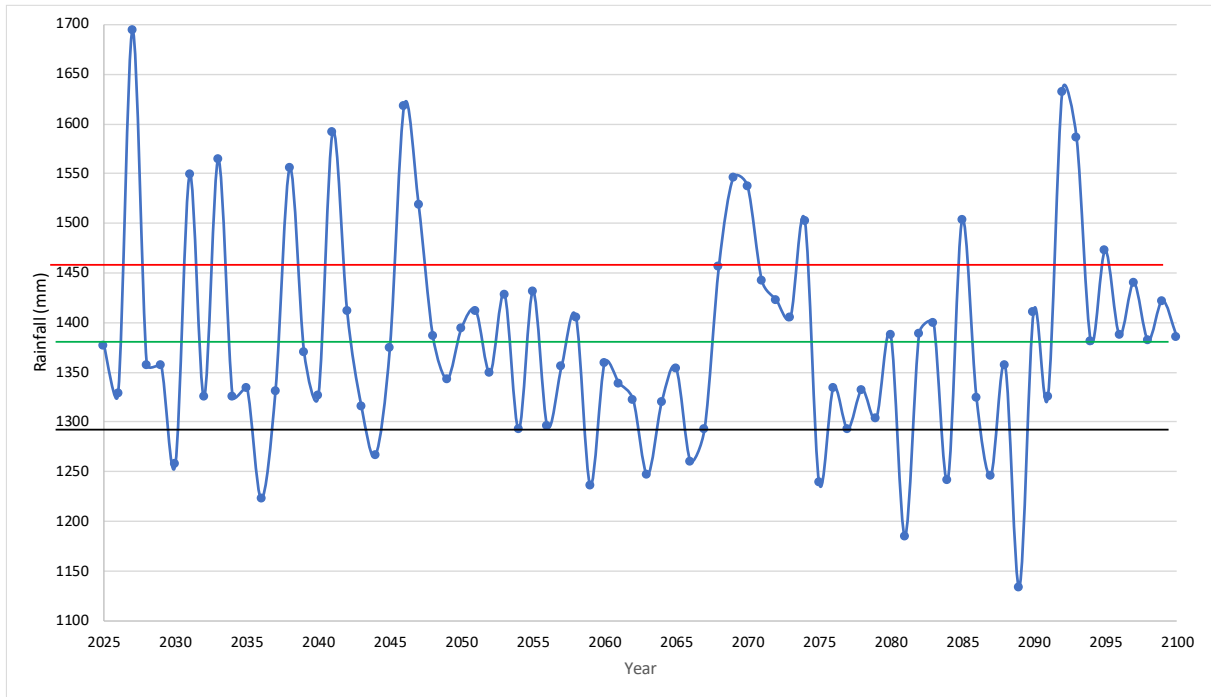
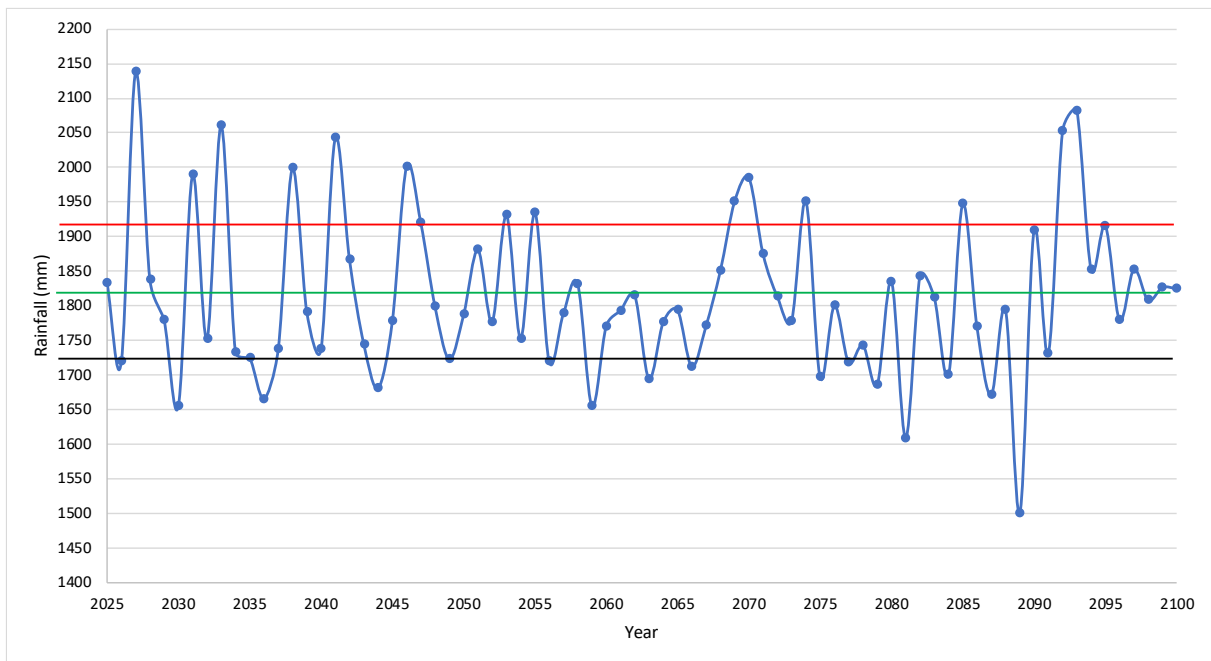


Figure 4. Predicted Rainfall in the Geres Daya Station



**Figure 5.** Predicted Rainfall in the Gunung Sari Station



**Figure 6.** Predicted Rainfall in the Keru Station

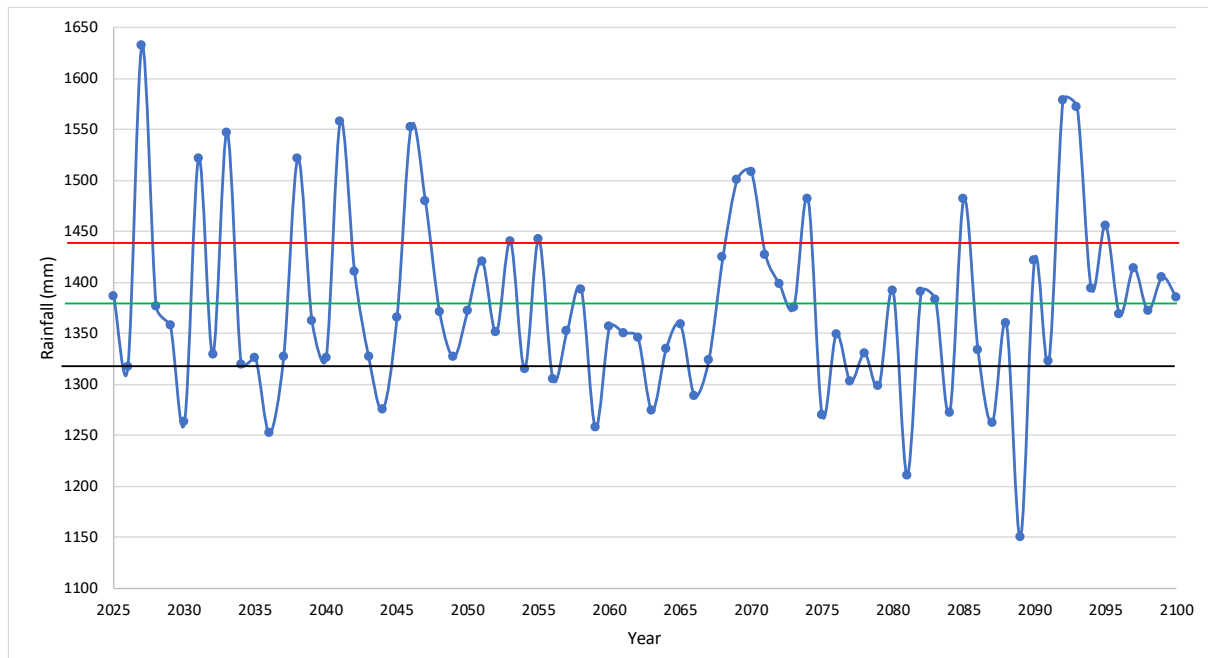


**Figure 7.** Predicted Rainfall in the Serumbung Station

Differences in predicted rainfall across the five stations can be explained by geographic and climatic factors. Dasan Cermen, which records the highest annual rainfall, is located near elevated terrain where orographic lifting enhances precipitation. In contrast, Geres Daya, further inland and in a relatively sheltered position, records the lowest rainfall totals, reflecting reduced exposure to moist air masses. Coastal stations such as Serumbung are influenced by maritime humidity and sea-land breeze circulations, which contribute to higher rainfall variability than at inland sites like Gunung Sari. Microclimatic conditions, including local vegetation cover and land use, also modulate rainfall intensity and distribution. These orographic, microclimatic, and coastal-inland contrasts underscore the importance of considering local geographic settings when interpreting rainfall projections and their implications for flood risk assessment.

### 2.3.7. Model Parameter Calibration

Figure 8 shows that the calibration of the hydrodynamic model for the urban coastal floodplain was conducted specifically for the Ancar River, as it was the only river that experienced flooding during the 06 June 2025 event. Manning's roughness coefficients were spatially varied to represent urban heterogeneity, with values of 0.006 for concrete-lined channels, 0.040 for mixed urban surfaces, and up to 0.060 for vegetated zones. Horizontal eddy viscosity was set at  $0.5 \text{ m}^2/\text{s}$ , while vertical mixing adopted a depth-uniform value of  $1\text{e-}3 \text{ m}^2/\text{s}$ . Structural elements such as culverts and weirs were parameterized with discharge coefficients of 0.70 and entrance/exit losses of 1.0, ensuring a realistic representation of hydraulic structures in the area of flooding. A tidal boundary condition of 0.5 m was imposed at the coastal edge,

providing stable forcing for surge-river interactions.

Boundary conditions were further fine-tuned with a +15% upstream discharge scaling and a +10% tidal amplitude adjustment to match peak depths and timing. Calibration achieved a water level RMSE below 0.20 m and an inundation extent F1-score exceeding 0.80. Importantly, the simulated flood extent closely matches observed inundation patterns in the observed views, confirming successful parameter tuning. This final configuration, focused on the Ancar River system, supports high-resolution flood forecasting and scenario testing under compound rainfall-tidal surge events, with stable CFL conditions and optimized grid nesting for critical flood-prone zones.

### 2.3.8. Flood Prediction

Flood predictions due to river overflows and the impact of tidal flooding are shown in Figure 9.

Based on the calibrated model parameters, the predicted flood extent across the coastal region was simulated using an expanded domain that includes all four major rivers—Meninting, Jangkok, Ancar, and Unus—as visualized in the attached flood depth map. The simulation captures spatial variations in inundation depth, with the western sector exhibiting higher flood levels, particularly near the Ancar River, which was the sole contributor to flooding during the 06 June 2025 event. The model integrates tidal forcing with a boundary level of 0.5 m, enabling realistic propagation of coastal surge into urban floodplains. The resulting flood patterns closely match observed inundation extents in both schematic and satellite views, validating the effectiveness of the parameter calibration and domain expansion.

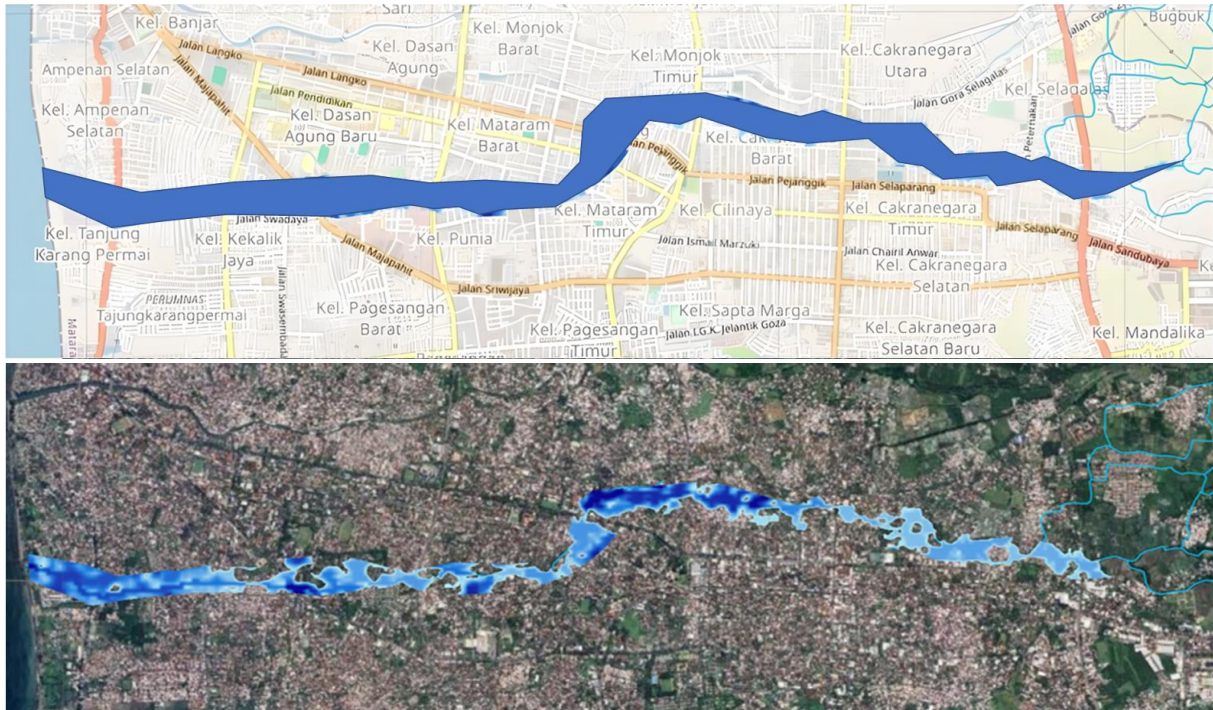


Figure 8. Calibration Process

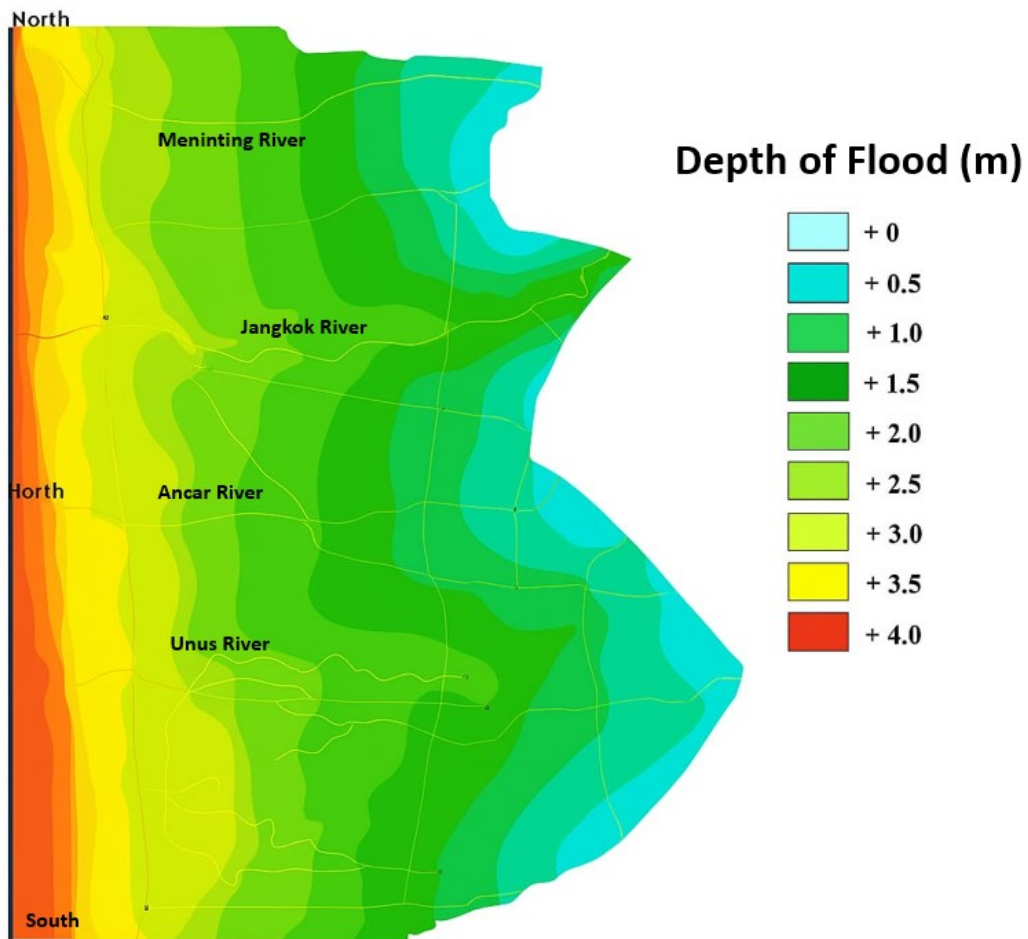


Figure 9. The Prediction of Maximum Flood in the Ampenan Coastal Area in 2100

Figure 9 further visualizes inland flood penetration and elevation changes across the Ampenan Coastal profiles under existing, 50-year, and 100-year scenarios. Simulations reveal significant long-term risks driven by sea level rise and extreme wave conditions, with flood propagation analyzed across seven coastal profiles. Inundated built-up areas increase from 5.09 ha in 2018 to 12.72 ha by 2118 under static land-use assumptions, and up to 65.57 ha under dynamic projections, equivalent to 1.07% of Mataram's total area. Inland flood penetration intensifies markedly, for instance, in Cross VI, flood extent grows from 81 m to 195 m, while wave elevation rises from 1.95 m to 2.4 m. Vulnerable zones such as Mapak Indah and the Ancar River corridor face recurrent tidal flooding, already impacting non-permanent housing. Although the study employs deterministic scenario-based simulations, the multi-horizon comparison offers transparent bounds on future flood risks. Incorporating probabilistic uncertainty bands remains a key recommendation for future research to enhance predictive robustness and inform long-term coastal planning.

### 3. Conclusions

This study advances climate risk science by introducing a hybrid downscaling framework that integrates regression analysis and artificial neural networks to improve the prediction of climate-induced disaster risks in coastal regions. Beyond methodological innovation, the framework delivers actionable outputs: high-resolution rainfall projections, inland tidal flood simulations, and geospatial hazard–exposure–vulnerability mapping. Applied to the Ampenan Coastal case, the results demonstrate practical utility for municipal planning, infrastructure investment, and community preparedness, while also strengthening inclusive risk communication and resilience strategies.

Several limitations must be acknowledged. The resolution of available climate and hydrologic data constrains fine-scale accuracy, and the relatively small number of monitoring stations introduces uncertainty in spatial rainfall variability. Assumptions embedded in the HEC-RAS hydraulic model, particularly boundary condition simplifications, may affect flood extent predictions. The ANN component carries risks of overfitting when trained on limited datasets, and land-use dynamics were treated as static, which reduces long-term realism.

These limitations highlight important pathways for future research. Incorporating multi-model ensembles could reduce uncertainty by leveraging complementary strengths of different downscaling and hydraulic approaches. The integration of advanced deep learning architectures, such as hybrid LSTM–ANN models, may improve temporal sequence prediction and capture long-term climate variability more effectively. Employing

finer-resolution digital elevation models (DEMs), enhanced by UAV or LiDAR data, would allow more accurate representation of micro-topography and floodplain dynamics. Finally, coupling hydrologic modeling with socio-economic exposure datasets would enable a more comprehensive assessment of flood risk, bridging physical hazard prediction with human vulnerability and resilience planning.

### Acknowledgements

The authors acknowledge the financial supports for this research from the University of Mataram, Indonesia and the Memorial University of Newfoundland, Canada. The acknowledgment is also going to the Big River Basin Organization for Nusa Tenggara I in Indonesia and the World Data Center Centre for Climate for providing the data.

### REFERENCES

- [1] Abbass K., Qasim M.Z., Song H., Murshed M., Mahmood H., Younis I., "A review of the global climate change impacts, adaptation, and sustainable mitigation measures," *Environmental Science and Pollution Research*, vol. 29, no. 39, pp. 42539–42559, 2022. DOI: 10.1007/s11356-022-19718-6.
- [2] Hattermann F.F., Krysanova V., "Impact attribution: exploring the contribution of climate change to recent trends in hydrological processes. An editorial introduction," *Climatic Change*, vol. 177, no. 1, pp. 172, 2024. DOI: 10.1007/s10584-024-03804-4.
- [3] Priestley R.K., Heine Z., Milfont T.L., "Public understanding of climate change-related sea-level rise," *PLoS ONE*, vol. 16, no. 7, pp. e0254348, 2021. DOI: 10.1371/journal.pone.0254348.
- [4] Bongarts Lebbe T., Rey-Valette H., Chaumillon É., Camus G., Almar R., Cazenave A., Claudet J., Rocle N., Meur-Férec C., Viard F., Mercier D., Dupuy C., M énard F., Rossel B.A., Mullineaux L., Sicre M-A., Zivian A., Gaill F., Euzen A., "Designing coastal adaptation strategies to tackle sea level rise," *Frontiers in Marine Science*, vol. 8, pp. 740602, 2021. DOI: 10.3389/fmars.2021.740602.
- [5] Guo W., Yao D., Chen Z., Ding P., Ge J., "Assessment of future flood risk induced by sea level rise and tropical cyclones under global warming in the Xiamen Bay, Fujian, China," *Frontiers in Marine Science*, vol. 10, pp. 1103279, 2023. DOI: 10.3389/fmars.2023.1103279.
- [6] Antara, "Climate change threatens small islands in West Nusa Tenggara," *ANTARA News*, <https://www.antaranews.com> (accessed Oct. 27, 2025).
- [7] Soesilo I., "Blue economy for marine resource development," *Eco-Business*, <https://www.eco-business.com> (accessed Oct. 27, 2025).
- [8] Yakin A., "*Analisis sumberdaya alam dan pembangunan*

*ekonomi berkelanjutan Propinsi NTB, Indonesia* (Analysis of natural resources and sustainable economic development of NTB Province, Indonesia)," Academia.edu, <https://www.academia.edu> (accessed Oct. 27, 2025).

- [9] IPCC, "First Assessment Report Overview and Policymaker Summaries and 1992 IPCC Supplement," IPCC, <https://www.ipcc.ch> (accessed Oct. 27, 2025)
- [10] Sulistiyono H., Saadi Y., Yasa I.W., "*Penelitian mengenai pengaruh perubahan iklim dan tataguna lahan terhadap sisa umur Bendungan Batujai* (Research on the influence of climate change and land use on the remaining life of the Batujai Dam)," Final Research Report, University of Mataram, 2015, pp. 1–80.
- [11] Sulistiyono H., Salehuddin, Suroso A., Harianto B., Setiawan A., "*Kajian pengaruh perubahan iklim dan fenomena El Niño terhadap karakteristik hujan di NTB* (Study of the influence of climate change and the El Niño phenomenon on rainfall characteristics in NTB)," Final Research Report, University of Mataram, 2017, pp. 1–90.
- [12] Sulistiyono H., Yasa I.W., Saidah H., Negara I.D.G.J., Setiawan E., "Impact of climate change and the El Niño–Southern Oscillation on extreme rainfall," *Environment and Ecology Research*, vol. 11, no. 2, pp. 284–294, 2023. DOI: 10.13189/eer.2023.110207.
- [13] Setiawan E., Sukarno S., Sulistiyono H., Pradjoko E., Pracoyo A., "Instrumentasi hidrologi untuk mendukung sistem monitoring peringatan dini banjir di Kota Mataram [Hydrological instrumentation to support the flood early warning monitoring system in Mataram City]," Final Research Report, University of Mataram, 2020, pp. 1–75.
- [14] Tabari, H., Mendoza Paz, S., Buekenhout, D., & Willems, P., "Comparison of statistical downscaling methods for climate change impact analysis on precipitation-driven drought," *Hydrology and Earth System Sciences*, vol. 25, no. 6, pp. 3493–3517, 2021. DOI: 10.5194/hess-25-3493-2021
- [15] Tian, D., & Wang, F., "Trend-preserving deep learning for multivariate bias correction and downscaling of climate models," *EGU General Assembly 2024*, 2024. DOI: 10.5194/egusphere-egu24-6408.